Some First Stars Were Red: Detecting Signatures of Massive Population III Formation through Long-term Stochastic Color Variations

Tyrone E. Woods[1,2], Chris J. Willott[1], John A. Regan[3], John H. Wise[4], Turlough P. Downes[5],
Michael L. Norman[6], and Brian W. O'Shea[7,8,9,10]

[1] National Research Council of Canada, Herzberg Astronomy & Astrophysics Research Centre, 5071 West Saanich Road, Victoria, BC V9E 2E7, Canada
tyrone.woods@nrc-cnrc.gc.ca, tewoods.astro@gmail.com
[2] Monash Centre for Astrophysics, School of Physics and Astronomy, Monash University, VIC 3800, Australia
[3] Department of Theoretical Physics, Maynooth University, Maynooth, Ireland
[4] Center for Relativistic Astrophysics, Georgia Institute of Technology, 837 State Street, Atlanta, GA 30332, USA
[5] Centre for Astrophysics & Relativity, School of Mathematical Sciences, Dublin City University, Glasnevin, D09 W6Y4, Ireland
[6] Center for Astrophysics and Space Sciences, University of California, San Diego, 9500 Gilman Drive, La Jolla, CA 92093, USA
[7] Department of Computational Mathematics, Science, and Engineering, Michigan State University, MI 48823, USA
[8] Department of Physics and Astronomy, Michigan State University, MI 48823, USA
[9] Joint Institute for Nuclear Astrophysics—Center for the Evolution of the Elements, USA
[10] National Superconducting Cyclotron Laboratory, Michigan State, University, MI 48823, USA

Abstract

Identifying stars formed in pristine environments (Population III) within the first billion years is vital to uncovering the earliest growth and chemical evolution of galaxies. Population III galaxies, however, are typically expected to be too faint and too few in number to be detectable by forthcoming instruments without extremely long integration times and/or extreme lensing. In an environment, however, where star formation is suppressed until a halo crosses the atomic-cooling limit (e.g., by a modest Lyman–Werner flux, high baryonic streaming velocities, and/or dynamical heating effects), primordial halos can form substantially more numerous and more massive stars. Some of these stars will in turn be accreting more rapidly than they can thermally relax at any given time. Using high-resolution cosmological zoom-in simulations of massive star formation in high-z halos, we find that such rapidly accreting stars produce prominent spectral features that would be detectable by the James Webb Space Telescope. The rapid-accretion episodes within the halo lead to stochastic reprocessing of 0%–20% of the total stellar emission into the rest-frame optical over long timescales, a unique signature which may allow deep observations to identify such objects out to $z \sim 10$–13 using mid- and wide-band NIRCam colors alone.

Unified Astronomy Thesaurus concepts: Population III stars (1285); Early universe (435); Primordial galaxies (1293)

1. Introduction

The first stars to have formed in the universe, though not yet detected, are canonically expected to have been extremely blue, with effective temperatures $T \sim 10^5$ K (Schaerer 2002; Murphy et al. 2021). This is due to their high masses and thus luminosities (Norman 2010), together with their compactness, which arises from the absence of metal-line opacity in their envelopes (Tumlinson & Shull 2000). These high temperatures, together with their high formation redshifts ($z \sim 10$–20) and the low efficiency of star formation expected in typical primordial halos, have conspired to temper expectations such Population III (Pop III) stars may be detected in pristine environments without prohibitively long exposures (e.g., Zackrisson et al. 2011).

However, while the first Pop III galaxies may go undetected, initial suppression of star formation in later primordial halos can ultimately lead to the formation of unusually massive Pop III stars (e.g., Bromm & Loeb 2003). The first Pop III stars to form did so in the shallow potential wells of the first virialized dark matter halos, with masses of $\sim 10^5$–10^6 $M_\odot$ (Abel et al. 2002). In these early structures, gas cools and contracts under the influence of cooling via vibrational and rotational transitions of H_2 (Tegmark et al. 1997). However, H_2 can be readily dissociated by Lyman–Werner (LW) radiation, suppressing initial star formation until the host halo reaches the atomic-cooling limit (Field et al. 1966; Haiman et al. 2000).

Cooling and consequently gravitational collapse can then be triggered by neutral hydrogen once the gas temperature reaches approximately 8000 K. A number of other mechanisms have also been found to suppress initial star formation and permit the formation of very massive or even supermassive stars, with individual stellar masses up to 10^5 $M_\odot$ (Woods et al. 2017, 2020; Lupi et al. 2021), including strong offsets between dark matter and baryonic streaming velocities within an environment (Tseliakhovich & Hirata 2010; Tanaka & Li 2014; Schauer et al. 2017), or strong dynamical heating either via major mergers (Mayer et al. 2010) or the rapid assembly of dark matter halos (e.g., Wise et al. 2019).

Recent numerical simulations have shown that a modest LW background, together with dynamical heating from minor and major mergers, can produce a primordial stellar population that is both much more numerous and more massive than that found in Pop III minihalos (Wise et al. 2019; Regan et al. 2020b). At the same time, the dense gas flows found in such an environment will lead to intermittent episodes of very rapid ($\gtrsim 0.005$ $M_\odot$ yr^{-1}) accretion for some stars. This is much faster than the rate at which such stars can thermally equilibrate, and will drive rapid photospheric expansion (Kippenhahn & Meyer-Hofmeister 1977; Haemmerlé et al. 2018), pushing the effective temperatures of these stars down to $\sim 5 \times 10^3$ K (Hosokawa et al. 2012) for the duration of the rapid-accretion phase. Therefore, in addition to a greatly enhanced total mass

formed in stars, we may also expect stochastic, and in some instances very strong, enhancements in the rest-frame optical continuum of these irradiated primordial halos, in particular at wavelengths longer than ∼4000 Å. This presents a uniquely promising opportunity for understanding primordial-composition stars in the early universe, allowing one to not only plausibly search for these stellar populations themselves but to characterize their formation environments at Cosmic Dawn.

2. Numerical Simulations

2.1. Halo Models

In order to compare the stellar populations of primordial halos, we draw on 3D hydrodynamic simulations of two primordial halos described in Regan et al. (2020b), which themselves were drawn from the original Renaissance simulations of Xu et al. (2013, 2014) and O'Shea et al. (2015), to which the interested reader is referred for further details. Halo A crosses the atomic-cooling limit before experiencing central gravitational collapse. This halo avoids star formation in its assembly history due to a combination of a mild LW ($J_{\mathrm{LW}} \sim (2\text{--}10) \times 10^{-21}$ erg s^{-1} cm^{-2} Hz^{-1} sr^{-1}) background and rapid halo assembly, which dynamically heats the halo, suppressing star formation prior to the onset of atomic cooling. Halo B, meanwhile, is not subjected to any LW background, and so star formation is governed by the presence of H_2, which allows the gas to cool and collapse, giving rise to a prototypical Pop III minihalo.

Here, we combine the results of these 3D radiation-hydrodynamics numerical simulations with postprocessing using a detailed spectral synthesis code, to produce model spectra for the two fiducial primordial Halos A and B. Using this pipeline, we then produce synthetic photometric magnitudes and colors, and demonstrate how Halo A can be detected and differentiated both from Halo B and more typical high-z galaxies. Finally, we outline detection prospects with forthcoming next-generation facilities such as the James Webb Space Telescope (JWST).

2.2. Fragmentation, Rapid Accretion, and Massive Star Formation

For our LW-irradiated model (Halo A), Regan et al. (2020b) found a $\gtrsim 70\times$ relative increase in the total mass of stars by the end of the simulation, with a mass spectrum peaking at $\sim 1000\ M_\odot$ and reaching $\sim 6000\ M_\odot$ (as opposed to stellar masses in the range $\sim 10\text{--}200\ M_\odot$ for our control case, Halo B). The final total mass (dark matter, gas, and stars) of Halo A was $M_{\mathrm{HaloA}} = 9.3 \times 10^7\ M_\odot$ (stellar mass: $\approx 90{,}000\ M_\odot$) and the final total mass of Halo B was $M_{\mathrm{HaloB}} = 3.7 \times 10^6\ M_\odot$ (stellar mass: $\approx 1{,}300\ M_\odot$).

Critically, the reason Halo A stars are unable to reach mass scales of order $\sim 10^5\ M_\odot$, which may however be possible in more strongly irradiated atomic-cooling halos (Lupi et al. 2021), is twofold. First, the gas readily fragments due to the presence of H_2 (Regan & Downes 2018) and second the protostars only intermittently intersect with pockets of dense infalling gas. The result is that truly rapid accretion ($\gtrsim 5 \times 10^{-3}\ M_\odot$ yr^{-1}) cannot be sustained, but arises only at random intervals in the lives of a fraction of the stars formed. The variation of this fraction with time for Halo A, along with the stellar mass evolution of both Halo A and Halo B, are plotted for a series of "snapshots" in Figure 1 (no stars enter
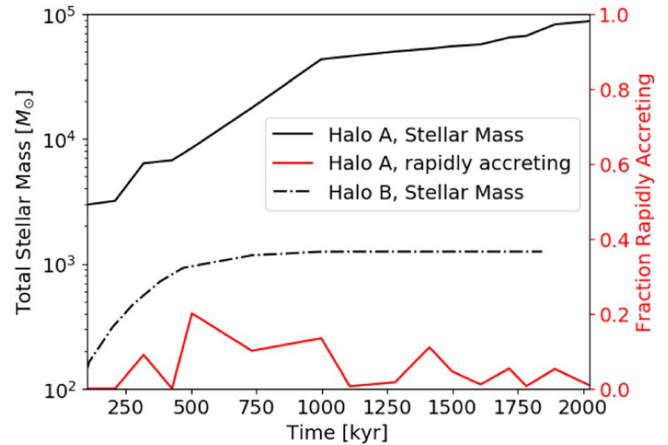

Figure 1. Total stellar mass formed (solid, black) and fraction of this mass in rapidly accreting stars (solid, red) as a function of time for Halo A. For comparison, the total mass formed in Halo B is also plotted (dotted–dashed, black), for which no stars are rapidly accreting.

such rapid-accretion phases in Halo B). As noted in Regan et al. (2020b), rapid growth will still greatly inflate the photospheres of those stars which are accreting. This has profound consequences for the anticipated spectra of these primordial stellar populations.

2.3. Postprocessing and Spectral Synthesis

For each snapshot, we assume that any stars not accreting above the "inflated photosphere" threshold ($\sim 5 \times 10^{-3}\ M_\odot$ yr^{-1}; Haemmerlé et al. 2018) are fully thermally relaxed. In this case, their spectral emission and temperatures are well described by blackbody emission with an effective temperature of $\approx 10^5$ K (Schaerer 2002; Woods et al. 2020). Stars growing at rates above this threshold, however, accrete much faster than they can thermally relax; the result is that their outer envelopes inflate dramatically (Kippenhahn & Meyer-Hofmeister 1977; Hosokawa et al. 2012), pushing their effective temperatures down to ~ 5000 K (Hosokawa et al. 2013). Here we assume all stars are simply either inflated or not at each snapshot based on their instantaneous accretion rate, given that the intervals between each snapshot are always much longer than the thermal timescale of any accreting star.

All of the stars we consider are massive (up to thousands of $M_\odot$); for simplicity, in the following we therefore assume that all stars in either halo radiate at approximately the Eddington limit, such that their luminosity is given by

$$L \approx 1.8 \times 10^{38} \times (M_*/M_\odot)\ \mathrm{erg\ s}^{-1}. \qquad (1)$$

Note that in practice, this may overestimate the luminosities for stars in Halo A by up to a factor of ~ 2, and by significantly more for the typically lower-mass stars in Halo B (Schaerer 2002). As shown below, however, Halo B remains too faint to be detected regardless; therefore, this does not significantly impact our results.

Once formed, these stars remain in a dense, gas-rich environment, and the effects of radiative transfer must be accounted for in order to produce a realistic model of their integrated emission. Here, we use the detailed plasma simulation and spectral synthesis code CLOUDY (version 17.02; Ferland et al. 2017), which solves for thermal and ionization equilibrium for arbitrary gas distributions, abundances, and source spectra in

1D. Although the restriction to 1D prevents us from precisely accounting for the clumpy medium seen in both halos, our focus on H and He lines within a modest density range, in an environment which is ionization bounded, prevents this from significantly impacting our results. We assume primordial composition (Planck Collaboration et al. 2014) and spherical symmetry, and derive ambient density profiles from our source simulations by taking spherical averages of the gas density at 0.5 pc intervals surrounding each star particle (see Regan et al. 2020b for further details). The spectrum of each star as filtered through its surrounding medium is then computed assuming dynamical and ionization equilibrium, and the resulting emission (including emission from the surrounding medium) is summed for all stars within each snapshot for Halo A and Halo B, respectively.

3. Observational Prospects

3.1. Synthetic Spectra

The total luminosity of Halo A grows throughout the ~ 2 Myr simulation (up to $\sim 10^{43}$ erg s^{-1}), tracing the evolution of the total stellar mass (recall Equation (1)) via both new star formation and accretion onto earlier-formed stars. The luminosity of Halo B, however, plateaus at $\sim 10^{41}$ erg s^{-1} after approximately 500 kyr (at which point both star formation and significant accretion end in Halo B). Both Halo A and Halo B exhibit comparably prominent hydrogen and helium emission lines, as expected for Pop III galaxies (Schaerer 2002). For instance, both halos exhibit rest-frame optical He II 4686 Å/Hβ ratios that typically fall around ~ 0.06, albeit with some very modest departures consistent with variations in the gas temperature and density seen between the two halos. This is consistent with the comparable ratios of H (13.6 eV) and He$^+$ (54.4 eV) ionizing photons between the two halos, although note that the ratio of ionizing photons to the mass of new stars formed, and thus the total luminosity of either line, varies stochastically in Halo A in response to the occurrence of rapid-accretion episodes for some stars (see below).

Other than the rapid growth in Halo A's luminosity, the most striking difference between Halo A and Halo B is the stochastic enhancement in the optical continuum of Halo A driven by the sporadic rapid-accretion episodes encountered by some of its stars. The net effect of accounting for the resulting photo-spheric expansion is that a variable but often significant fraction of the total luminosity of the halo (between 0% and 20% in the case of our Halo A simulation) is reprocessed from the extreme UV to the optical. This may be contrasted with, e.g., the typical $\sim 3\%$ of any $T \sim 10^5$ K object's luminosity that is reprocessed into Hα, the strongest rest-frame optical line, under the conditions prevailing in our simulations. The emergent spectrum from these rapidly accreting objects contributes to a broad continuum enhancement, particularly at wavelengths above ~ 4000 Å. A relatively extreme example of this is shown in Figure 2, where a $\sim$fivefold continuum enhancement is seen early in the evolution of Halo A as it transitions from a quiescent moment to a resumption of rapid growth.

3.2. Photometric Magnitudes and Colors with Redshift

In the near-term, the ideal instrument for accessing the rest-frame optical at high redshifts, with sufficient sensitivity and spatial resolution, is JWST. In order to produce synthetic
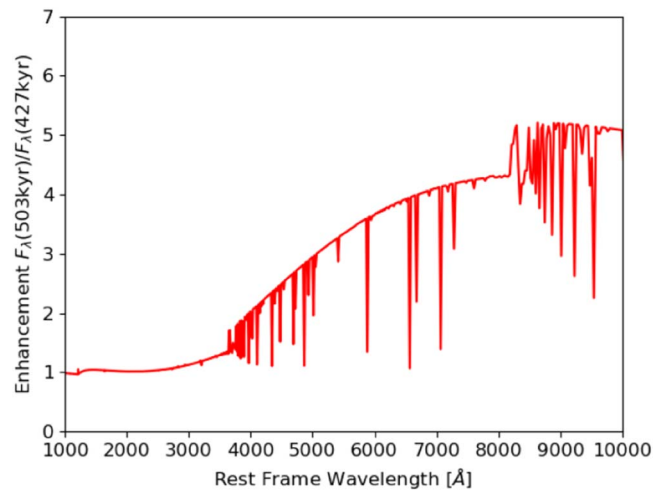

Figure 2. Enhancement in the rest-frame UV, optical, and near-IR spectral energy distribution of our model halo ("Halo A") at 503 kyr (when many stars are rapidly accreting) relative to the case at 427 kyr (a quiescent moment).
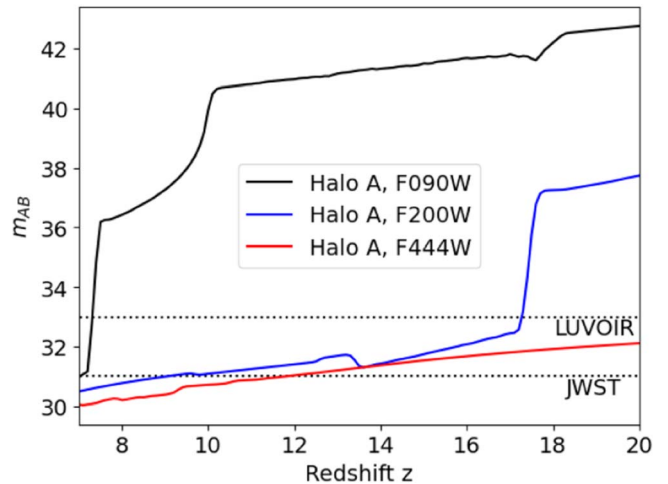

Figure 3. Wide-band AB magnitudes for the F200W (blue) and F444W (red) NIRCam filters shown as a function of assumed redshift, for Halo A at 1892 kyr (note that here and throughout, we take a single simulation and redshift its rest-frame spectrum accordingly). Also shown for reference is the Lyman-limit dropout above $z \sim 7$, as seen in the F090W band (black). Horizontal dotted black lines denote a marginal detection with an S/N ~ 5 for JWST and LUVOIR after ~ 17 and ~ 10 hr integrations, respectively.

observed magnitudes based on our model spectra, we use the software package SYNPHOT[11] (STScI Development Team 2018). Note that while the simulations of both Halo A and Halo B found the onset of star formation to arise at $z \sim 15$, a broad range of formation redshifts are possible depending on the availability of metal-free gas in an appropriate environment (Regan et al. 2020a).

The simulated F200W and F444W magnitudes near the end of the simulation for Halo A are shown in Figure 3, as a function of the assumed formation redshift (as well as the F090W band, which illustrates the Lyman-limit dropout for $z \gtrsim 7$). Remarkably, the strongly enhanced star formation efficiency and stellar accretion within Halo A renders it detectable at modest redshifts, given long yet plausible integration times, e.g., for a F444W AB magnitude = 31, NIRCam would reach a signal-to-noise ratio (S/N) ~ 5 in a 17 hr observation in a low

---

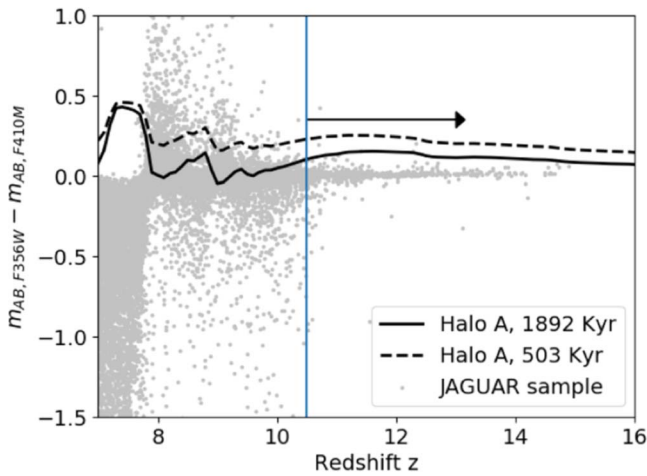[11] https://synphot.readthedocs.io/en/latest/

3

Figure 4. Observed NIRCam F356W–F410M color of Halo A as a function of the redshift assumed for snapshots at 503 kyr (dashed; rapidly accreting) and 1892 kyr (solid; final). Shown for comparison is the same NIRCam color for the JAGUAR mock catalog of expected JWST high-z sources. The vertical bar highlights the approximate redshift ($z \sim 10.5$) above which stochastic reddening can provide a distinct color signature of rapidly accreting Pop III stars.

background field (JWST Exposure Time Calculator[12]), allowing JWST to detect objects like Halo A out to $z \sim 12$. Future proposed missions, such as the Large UV/Optical/Infrared Surveyor (LUVOIR) mission concept, would be able to extend this to $z \sim 17$, reaching a planned S/N ~ 5 in ~ 10 hr (The LUVOIR Team 2019). This is in stark contrast with Halo B; even when assuming the Eddington luminosity for all stars, Halo B only reaches $m_{AB} \sim 35$ by the end of its evolution assuming formation at $z \sim 7$. Typical for Pop III halos, then, Halo B would only be detectable, even given next-generation facilities, with the benefit of extreme lensing (e.g., Zackrisson et al. 2012).

The faintness and uncertain number density of objects like Halo A, however, necessitates a search strategy that does not initially rely on time-intensive high-S/N spectroscopy. The question then arises whether such objects could be identified by their broadband and mediumband photometric colors alone. The dense inflowing gas and stochastically arising rapid-accretion episodes within Halo A lead to pronounced episodes of reddening over the lifetime of the starburst, in sharp contrast to Halo B. This suggests that rapidly accreting Pop III stars may be distinguished from more typical Pop III minihalos based on color alone. Shown in Figure 4 is the color of two snapshots of Halo A plotted as a function of redshift. For comparison, we also plot the same colors for simulated star-forming galaxies from the JAdes extraGalactic Ultradeep Artificial Realizations (JAGUAR) package (Williams et al. 2018).

The redder continuum of these models shows up as a broad excess approximately 0.1–0.3 magnitudes redder than the locus of the JAGUAR models in a number of JWST NIRCam colors, e.g., at $z \sim 10.5$–13 for F356W–F410M. Note that differentiating colors to such a precision would require a $\sim 10\sigma$ detection, necessitating either extremely long integrations or more modestly deep observations of lensed environments. Critically, since the majority of Halo A's emission remains in the blue, such objects could still be identified as high-z (and in particular,

disambiguated from brown dwarfs and other low-z objects) based on their Lyman dropout (see, e.g., the predicted F090W magnitudes in Figure 3, which show a Lyman-limit cutoff for $z \gtrsim 7$). At lower redshifts ($7 \lesssim z \lesssim 8$), the narrower, deeper feature opposite to the JAGUAR locus is due to Hβ being within the filter for the model halo, whereas there is stronger [O III] 5007 Å emission in the neighboring filter for the JAGUAR mock galaxies; such behavior is generic for any metal-free stellar population with strong Balmer lines (Zackrisson et al. 2011).

4. Discussion

Although it is clear objects such as Halo A may be detectable by JWST, the question remains whether or not they will be sufficiently numerous to be found given JWST's relatively small footprint. Here, we may make some indicative estimates from comparison with previous studies of supermassive star formation rates (see, e.g., Woods et al. 2019 for a review). The critical conditions needed for supermassive star formation in primordial halos were long approximated as a single threshold Lyman–Werner intensity within the ambient environment (Bromm & Loeb 2003), although recent work suggests a realistic treatment is considerably more nuanced (e.g., Sugimura et al. 2014; Agarwal et al. 2016; Wolcott-Green et al. 2017). Estimates for the critical Lyman–Werner intensity needed for supermassive star formation have varied widely, with consequently wide variation in their expected number densities, e.g., for $J_{crit} \sim 30 J_{LW}$, Agarwal et al. (2012) find $\sim 10^{-2}$–10^{-1} cMpc^{-3} at $z \sim 10$, whereas Dijkstra et al. (2008) found only $\sim 10^{-6}$ cMpc^{-3} for $J_{crit} > 1000 J_{LW}$. A number of other factors, however, including dynamical heating (e.g., Wise et al. 2019) and baryonic streaming velocities (e.g., Tanaka & Li 2014), may also contribute to suppressing typical star formation in primordial halos, providing complementary means for seeding supermassive stars that may imply greater number densities.

The conditions needed for simply enhancing the total mass, individual stellar masses, and stochastic accretion rates within Pop III halos, as seen above, appear to be similar if more modest. In the case of Halo A, the key factor was found to be dynamical heating caused by the rapid assembly of the halo, more than the moderate ambient LW background (Wise et al. 2019; Regan et al. 2020b). This rapid assembly heats the halo, similarly delaying and suppressing star formation. Wise et al. (2019) calculated the number density of such halos to be approximately $\sim 1 \times 10^{-3}$ cMpc^{-3} at $z \sim 15$, suggesting an occurrence rate as high as $\sim$ a few per NIRCam field of view (for $\Delta z = 1$). The region in which the parent simulations were run, however, was an overdense region (see, e.g., Xu et al. 2013), and when this is accounted for the total expected number density over the whole sky falls to $\sim 1 \times 10^{-6}$ cMpc^{-3} at $z \sim 15$ (e.g., ~ 1 per 200 NIRCam pointings, and consistent with Dijkstra et al. 2008). The formation rate of such objects in "normal" (as opposed to overdense) regions is expected to rise significantly at lower redshifts, however, at least up to $z \sim 10$–12 (e.g., Regan et al. 2020a); beyond this point, increasing metal pollution may hinder the rise of pristine atomic-cooling halos at still lower redshifts, though this remains poorly constrained.

Ultimately, our analysis represents only a single simulation, and the real abundance of similarly enhanced Pop III halos cannot be reliably estimated without a greater understanding of the relative importance of LW irradiation (including in

synchronized halos; e.g., Regan et al. 2017), dynamical heating from mergers, and baryonic streaming velocities in producing such populations in average-density regions of the early universe, which is beyond the scope of the present work. We may argue, however, that depending on the real evolving number density as a function of redshift:

1. If objects such as Halo A continue to form up until $z \sim 7$–8, then planned observations such as the JADES GTO program (whose deep survey will reach an S/N ~ 10 for AB mag ~ 30; Williams et al. 2018) will be able to detect similar objects and identify them by their color.

2. If Halo A-like objects only form at $z \gtrsim 10$, then robustly detecting them without the benefit of lensing would be too time-intensive for blind surveys (e.g., reaching S/N ~ 10 for $z \sim 12$ objects would require ~ 68 hr on JWST). Shallow or pure parallel surveys with JWST, however, should soon reveal overdensities at $z \sim 10$, as will deep surveys with, e.g., the Roman Space Telescope (Vikaeus et al. 2021). These overdensities may then be targeted for deep follow-up observations.

3. If the true number density of Halo A-like objects is significantly greater than our estimate based on expected supermassive star formation sites, it may be viable to search for lensed objects even in untargeted surveys. For example, we note that in the CANUCS survey, we expect 10 arcmin^2 within its planned footprint to have a magnification $\gtrsim 3$–4 (C. Willott 2021, private communication). This suggests such an approach may be able to detect (or rule out) formation rates of Halo A-like objects consistent with the very highest number densities of such halos.

4. Finally, if the formation rate of Halo A-like objects is significantly lower than our estimates given above, or if they arise only at higher redshifts (e.g., $z \gtrsim 15$), such objects may yet be revealed by next-generation facilities such as the proposed LUVOIR mission (recall Figure 3).

5. Conclusion

Here we have shown that rapidly accreting Pop III stars, arising in pristine environments wherein star formation was initially suppressed, may have a profound influence on the spectral features and color of some primordial stellar populations. In particular, chance encounters between Pop III stars and dense gas within such halos will lead to rapid-accretion episodes that will greatly inflate the photospheres of these stars, potentially reprocessing a significant fraction of the halo's total stellar emission to the rest-frame optical. Together with the highly enhanced star formation indicated by our models in such environments, we have shown that such populations would be detectable by forthcoming next-generation infrared facilities, and distinguishable from more typical, metal-enriched stellar populations at $z \gtrsim 10.5$ and at $7 \lesssim z \lesssim 8$ based on their broadband and mediumband colors alone. Conversely, this stochastically arising reddening of some Pop III halos may provide an invaluable probe of the star formation history and environment in overdense regions of the early universe, providing a direct probe of the total mass in rapidly accreting and quiescent states within such early populations.

ORCID iDs

Tyrone E. Woods ● https://orcid.org/0000-0003-1428-5775
Chris J. Willott ● https://orcid.org/0000-0002-4201-7367
John A. Regan ● https://orcid.org/0000-0001-9072-6427
John H. Wise ● https://orcid.org/0000-0003-1173-8847
Turlough P. Downes ● https://orcid.org/0000-0002-7639-5446
Michael L. Norman ● https://orcid.org/0000-0002-6622-8513
Brian W. O'Shea ● https://orcid.org/0000-0002-2786-0348

References

Abel, T., Bryan, G. L., & Norman, M. L. 2002, Sci, 295, 93
Agarwal, B., Khochfar, S., Johnson, J. L., et al. 2012, MNRAS, 425, 2854
Agarwal, B., Smith, B., Glover, S., Natarajan, P., & Khochfar, S. 2016, MNRAS, 459, 4209
Bromm, V., & Loeb, A. 2003, ApJ, 596, 34
Dijkstra, M., Haiman, Z., Mesinger, A., & Wyithe, J. S. B. 2008, MNRAS, 391, 1961
Ferland, G. J., Chatzikos, M., Guzmán, F., et al. 2017, RMxAA, 53, 385
Field, G. B., Somerville, W. B., & Dressler, K. 1966, ARA&A, 4, 207
Haemmerlé, L., Woods, T. E., Klessen, R. S., Heger, A., & Whalen, D. J. 2018, MNRAS, 474, 2757
Haiman, Z., Abel, T., & Rees, M. J. 2000, ApJ, 534, 11
Hosokawa, T., Yorke, H. W., Inayoshi, K., Omukai, K., & Yoshida, N. 2013, ApJ, 778, 178
Hosokawa, T., Yoshida, N., Omukai, K., & Yorke, H. W. 2012, ApJL, 760, L37
Kippenhahn, R., & Meyer-Hofmeister, E. 1977, A&A, 54, 539
Lupi, A., Haiman, Z., & Volonteri, M. 2021, MNRAS, 503, 5046
Mayer, L., Kazantzidis, S., Escala, A., & Callegari, S. 2010, Natur, 466, 1082
Murphy, L. J., Groh, J. H., Ekström, S., et al. 2021, MNRAS, 501, 2745
Norman, M. L. 2010, in AIP Conf. Ser., 1294, The First Stars and Galaxies: Challenges for the Next Decade, ed. D. J. Whalen, V. Bromm, & N. Yoshida (Melville, NY: AIP), 17
O'Shea, B. W., Wise, J. H., Xu, H., & Norman, M. L. 2015, ApJL, 807, L12
Planck Collaboration, Ade, P. A. R., Aghanim, N., et al. 2014, A&A, 571, A16
Regan, J. A., & Downes, T. P. 2018, MNRAS, 475, 4636
Regan, J. A., Visbal, E., Wise, J. H., et al. 2017, NatAs, 1, 0075
Regan, J. A., Wise, J. H., O'Shea, B. W., & Norman, M. L. 2020a, MNRAS, 492, 3021
Regan, J. A., Wise, J. H., Woods, T. E., et al. 2020b, OJAp, 3, 15
Schaerer, D. 2002, A&A, 382, 28
Schauer, A. T. P., Regan, J., Glover, S. C. O., & Klessen, R. S. 2017, MNRAS, 471, 4878
STScI Development Team 2018, synphot: Synthetic Photometry using Astropy, Astrophysics Source Code Library, ascl:1811.001
Sugimura, K., Omukai, K., & Inoue, A. K. 2014, MNRAS, 445, 544
Tanaka, T. L., & Li, M. 2014, MNRAS, 439, 1092
Tegmark, M., Silk, J., Rees, M. J., et al. 1997, ApJ, 474, 1
The LUVOIR Team 2019, arXiv:1912.06219
Tseliakhovich, D., & Hirata, C. 2010, PhRvD, 82, 083520

Tumlinson, J., & Shull, J. M. 2000, ApJL, 528, L65
Vikaeus, A., Zackrisson, E., Schaerer, D., et al. 2021, arXiv:2107.01230
Williams, C. C., Curtis-Lake, E., Hainline, K. N., et al. 2018, ApJS, 236, 33
Wise, J. H., Regan, J. A., O'Shea, B. W., et al. 2019, Natur, 566, 85
Wolcott-Green, J., Haiman, Z., & Bryan, G. L. 2017, MNRAS, 469, 3329
Woods, T. E., Agarwal, B., Bromm, V., et al. 2019, PASA, 36, e027
Woods, T. E., Heger, A., & Haemmerlé, L. 2020, MNRAS, 494, 2236

Woods, T. E., Heger, A., Whalen, D. J., Haemmerlé, L., & Klessen, R. S. 2017, ApJL, 842, L6
Xu, H., Ahn, K., Wise, J. H., Norman, M. L., & O'Shea, B. W. 2014, ApJ, 791, 110
Xu, H., Wise, J. H., & Norman, M. L. 2013, ApJ, 773, 83
Zackrisson, E., Rydberg, C.-E., Schaerer, D., Östlin, G., & Tuli, M. 2011, ApJ, 740, 13
Zackrisson, E., Zitrin, A., Trenti, M., et al. 2012, MNRAS, 427, 2212